Extensive validation of the SSI macro element using experimental and numerical results

Stéphane Grange, Panagiotis Kotronis, Jacky Mazars

Project No.: GOCE-CT-2003-505488

LESSLOSS

Risk Mitigation for Earthquakes and Landslides
Integrated Project

Sixth Framework Programme

Priority 1.1.6.3 Global Change and Ecosystems

Deliverable Report

Deliverable [D8-2] – Extensive validation of the SSI macro element using experimental and numerical results

Sub-Project 8 – Displacement-based Design Methodologies

Deliverable/Task Leader: INPG Revision: Final

March, 2007

Project co-funded by the European Commission within the Sixth Framework Programme (2002-2006)		
Dissemination Level		
PU	Public	X
PP	Restricted to other programme participants (including the Commission Services)	
RE	Restricted to a group specified by the consortium (including the Commission Services)	
CO	Confidential, only for members of the consortium (including the Commission Services)	

PREFACE

A 3D "macro element" which allow taking into account Soil-Structure Interaction (SSI) has been presented in the deliverable number 67 of the LESSLOSS project [Grange *et al.,* 2006a]. This new macro-element permits to reproduce the behaviour of a circular and rigid foundation considering rocking and the plasticity of the soil.

In order to validate and to prove the good performance of this element extensive simulations are presented in this report. They concern the numerical modelling of a seven story building tested on a shaking table considering different boundary conditions. At first, the structure is supposed embedded in the shaking table and is discretised using multifiber Timoshenko beams. Further simulations are made considering SSI and different types of soils or base isolators.

It is shown that the proposed modelling strategy describes accurately the global behaviour of the structure and qualitatively the distribution of damage for all different configurations. Based on the results obtained it appears now possible to use this approach to investigate numerically the behaviour of a wider variety of configurations.

ACKNOWLEDGEMENTS

The work presented in this deliverable has been undertaken in Institut National Polytechnique de Grenoble (INPG) – Laboratory 3S-R by PhD student Stéphane Grange, Assist. Prof. Panagiotis Kotronis and Prof. Jacky Mazars.

The authors would like to congratulate the organizers of the seven-story building-slice earthquake blind prediction contest and to thank them for their financial support that made possible for the 3S-R group to participate to the NEES/UCSD Workshop and Seminar "Analytical Model of Reinforced Concrete Walls" held in San Diego the 15th and 16th of December 2006.

TABLE OF CONTENTS

LIST OF TABLES

LIST OF FIGURES

LIST OF SYMBOLS AND ABBREVIATIONS

a,b,c,d,e,f = Parameters defining the shape and the size of the loading surface and the failure criterion;

D = Diameter of the foundation;

K^{el} = Elastic tangent stiffness matrix;

q_{max} = Ultimate pressure of the foundation under vertical centre load;

a_1 = 1st parameter governing the evolution of damage (traction) for concrete;

a_2 = 1st parameter governing the evolution of damage (compression) for concrete;

a_3 = coefficient for isotropic hardening in compression for steel;

a_4 = coefficient for isotropic hardening in tension for steel;

b = hardening ratio for steel;

b_1 = 2nd parameter governing the evolution of damage (traction) for concrete;

b_2 = 2nd parameter governing the evolution of damage (compression) for concrete;

E_0 = initial Young modulus for steel;

E_c = initial Young modulus for concrete;

f'_c = ultimate compressive stress for concrete;

f_{su} = ultimate stress for steel;

f_t = ultimate tensile stress for concrete;

f_y = yield stress for steel;

I_{fz} = mass inertia of the flange wall nodes;

I_{wz} = mass inertia of the web wall nodes;

$ID_{i,i+1}$ = interstory drift between floor i and i + 1;

y_{01} = initial damage threshold for concrete (traction);

y_{02} = initial damage threshold for concrete (compression);

M_i = overturning moment at level i;

M_{fi} = mass of the flange wall at node i;

M_{wi} = mass of the web wall at node i;

u_{Y1} = displacement of node i of the web wall according to Y axis;

$\ddot{u}_{Y1}$ = acceleration of node i of the web wall according to Y axis;

V_i = shear force at level i;

X_i = distance of node i from the base of the structure;

β_1 = anelastic parameter for traction for concrete;

β_2 = anelastic parameter for compression for concrete;

ε_{cu} = ultimate compressive strain for concrete;

ε_{sh} = yield strain for steel;

ε_{su} = ultimate strain for steel;

σ_{f1} = crack closure stress for concrete;

ν = Poisson coefficient for the soil;

ν_b = Poisson coefficient for concrete.

1. INTRODUCTION

In structural engineering, Soil-Structure Interaction (SSI) is an important phenomenon that must be taken into account. When designing slender structures like buildings or bridge piers it is necessary to define the characteristics of the soil, the structure and the nature of the connection between them. It is evident that the behaviour would be different if the structure is embedded in the soil or just connected with a knee joint [Crémer, 2001].

In order to study the effects of SSI or other types of boundary conditions (as base isolators) a new 3D macro element has been developed [Grange *et al.,* 2006a], [Grange *et al.,* 2007a], [Grange *et al.,* 2007b]). This new macro element permits to reproduce the behaviour of a circular and rigid foundation considering rocking and the plasticity of the soil.

In order to validate and to prove the good performance of this macro element extensive simulations are presented in this report. They concern the numerical modelling of a seven story building tested on a shaking table. The tests have been made by the University of California at San Diego (UCSD), the Portland Cement Association (PCA) of Skokie, IL. and the NEES Consortium Inc (NEESinc) [NEES7story, 2006]. They realised a seismic research project around a uniaxial shaking table test on a mock-up representing a full-scale vertical slice of a seven-story reinforced concrete wall building. The structure is composed of two perpendicular walls linked with slotted connections. The building slice was designed using a displacement-based and capacity approach for a site in Los Angeles.

For the first calculations presented in this report the structure is supposed embedded in the shaking table. Multifiber Timoshenko beam elements are used to reproduce numerically the behaviour of the structure. Simulations are performed with FedeasLab, a finite element Matlab toolbox, developed by Pr. F. Filippou and his co-workers in UC Berkeley [Filippou *et al.,* 2004]. The Timoshenko multifiber beam element and the damage mechanics law used for concrete have been introduced into FedeasLab by the 3S-R group. A comparison between the behaviour of the embedded structure and the structure considering SSI for different types of soils via the 3D macro element follows. Finally, the influence of the dissipative behaviour of base isolators on the behaviour of the specimen is also reproduced numerically.

2.SEVEN-STORY BUILDING-SLICE EARTHQUAKE BLIND PREDICTION CONTEST: A SIMPLIFIED MODELING USING MULTIFIBER TIMOSHENKO BEAMS

This first part of the report presents the work of the team of the Laboratory Sols Solides Structures-Risques (3S-R) in Grenoble in France concerning the benchmark NEES/UCSD performed between October 2005 and January 2006 [NEES7story, 2006]. The aim is to model a full-scale vertical slice of a seven-story reinforced concrete walls building (Figure 2.1) subjected to increasing intensity of uniaxial earthquake ground motions on the new NEES Large High-Performance Outdoor Shake Table.

The structure is composed of 2 main perpendicular walls: the web wall and the flange wall linked with the slabs. It is considered embedded in the shaking table. A pre-cast column needed to limit torsional behaviour and gravity columns to support slabs are also present. The building slice was designed using a displacement-based and capacity approach for a site in Los Angeles resulting in design lateral forces that are significantly smaller than those currently specified in building codes used in the United States. Only the direction Y of loading is considered (parallel to the web wall). Four input motions at different intensities have been used coming from the Sylmar Medical Facility free-field record obtained during the 1994 Northridge Earthquake.

The results presented in this section and the comparisons with the experimental response are "blind". The building is modelled using Timoshenko multifiber beam elements ([Kotronis *et al.,* 2005] and [Mazars *et al.,* 2006]). Constitutive material laws are based on damage mechanics to describe cracking of concrete [La Borderie, 1991] and on plasticity for steel ([Menegoto *et al.,* 1973] as modified by Pr. Filippou of UC Berkeley with an isotropic hardening). The Timoshenko multifiber beam element and the damage mechanic law have been introduced into FedeasLab, a Matlab finite element toolbox [Filippou *et al.,* 2004] by the 3S-R group. We present hereafter in details the mesh, the material parameters and the response of the numerical model compared with the experimental results.

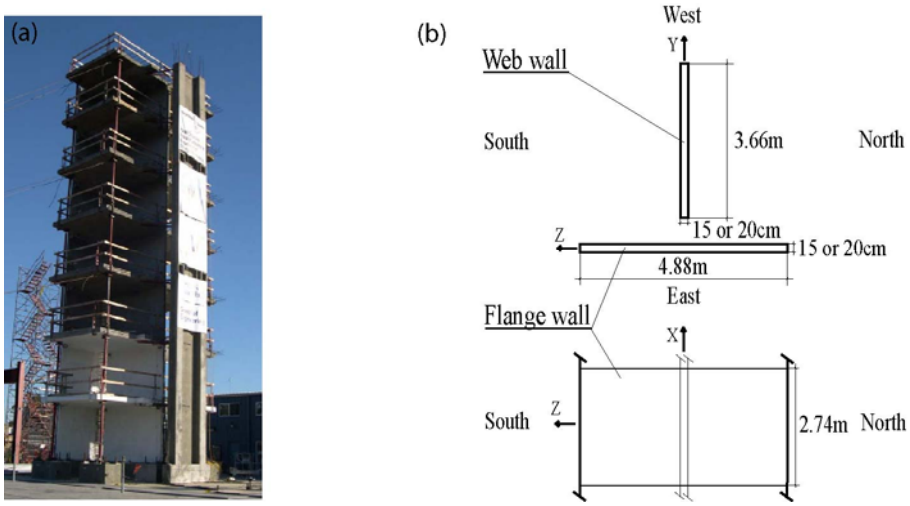

Figure 2.1. (a) North West view of the mock up [NEES7story, 2006] and (b) Geometrical data of the mock up.

2.1 NUMERICAL MODEL OF THE SEVEN-STORY BUILDING

2.1.1 Spatial discretization

A good comprehension of the role of each structural element is important in order to choose the correct finite element mesh of the structure. The building is made of a web wall and a flange wall connected by slotted connections. They constitute the main skeleton of the structure supporting the seven slabs. Gravity columns permit to support the weight of the slabs and they are positioned at their extremities. The dynamic solicitation is applied toward the Y direction only (in the plane of the web wall, see Figure 2.2). In order to avoid any 3D effects and particular any torsional mode, pre-cast segmental piers (PT columns) as well as bracing are used.

The dynamic solicitation being unidirectional, the gravity columns, the pre-cast segmental pier and the bracing system are not taken into account into the numerical model presented hereafter. Figure 2.2 (a) gives a representation of the finite element discretization. The web wall and the flange wall are decomposed into 19 multifiber Timoshenko beam elements (4 elements for levels 1 and 2, 3 elements for level 3 and 2 elements for levels 5, 6 and 7). The slotted connections are simulated using linear bar elements. 4 linear Bernoulli beam elements are used to reproduce the shaking table.

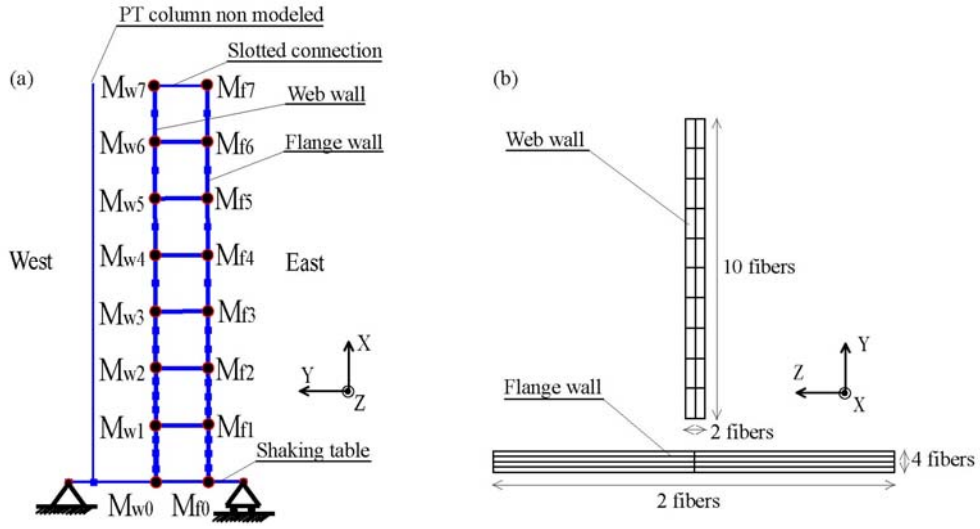

Figure 2.2. (a) Finite element mesh and concentrated masses and (b) fibers in a given section.

2.1.2 Distribution of masses

Concentrated masses are considered at each floor taking into account the mass of the corresponding slab and the upper and lower part of the wall. They are presented in Table 2.1, Table 2.2 and Figure 2.2 (a).

Table 2.1. Masses and rotational inertia for the nodes in the web wall

Node	Masses M_w (kg)	Rotational inertia I_{wz} (kg.m2)
w_0	11780	20080
w_1	18470	23100
w_2	17910	22000
w_3	17910	22000
w_4	17910	22000
w_5	17910	22000
w_6	17910	22000
w_7	16200	22000

Table 2.2. Masses and rotational inertia for the nodes in the flange wall

Node	Masses M_f (kg)	Rotational inertia I_{fz} (kg.m2)
f_0	15500	5499
f_1	5376	3582
f_2	4576	3071
f_3	4576	3071
f_4	4576	3071
f_5	4576	3071
f_6	4576	3071
f_7	2126	1535

2.1.3 Behaviour of the materials

Constitutive model for concrete under cyclic loading ought to take into account some observed phenomena such as decrease in material stiffness due to cracking, stiffness recovery which occurs at crack closure and inelastic strains concomitant to damage. To simulate this behaviour we use a uniaxial damage model with two scalars variables, one in compression and one in tension [La Borderie, 1991] (shear is considered linear). Inelastic strains are taken into account thanks to an isotropic tensor (Figure 2.3).

A modified version of the classical Menegoto-Pinto model [Menegoto and Pinto, 1973], [Filippou *et al.,* 1983] with an isotropic hardening is used for steel. Specific parameters for each model are presented in Table 2.3.

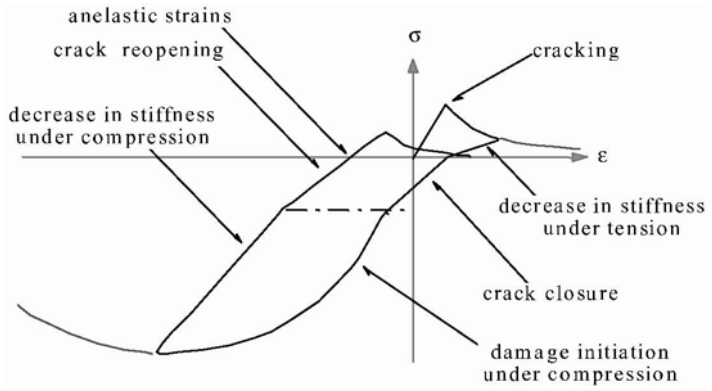

Figure 2.3. 1D cyclic response of the La Borderie Model.

2.1.4 Material data parameters

The material data parameters of concrete and steel are fitted using the values provided in the contest rules. To simplify the problem only one type of concrete (concrete specimen number "c3", [NEES7story, 2006]) and steel are adopted. An ultimate compressive stress of f_c = 37.4MPa (= 5.43ksi) for a compressive strain of ε_{cu} = 0.00259 is chosen and the Young modulus is taken equal to E_c = 24.46GPa (= 3549ksi). In traction, the ultimate stress is f_t = 3MPa (= 0.43ksi) according to the empirical French rule (f_t = 0.6+0.06f_c) [BAEL91, 2000]. The ultimate stress and yield stress for steel are taken equal to f_{su} = 710MPa (= 103ksi) and f_y = 450MPa (= 65.3ksi) respectively. The corresponding ultimate strain and yield strain are ε_{su} = 0.10, and ε_{sh} = 0.0060. Theses values lead to the material data parameters presented in Table 2.3.

2.1.5 Multifiber sections

The multifiber elements composing the web wall are divided into 20 concrete fibres whereas those of the flange wall are divided into 8 concrete fibres (Figure 2.2 (b)). The number and the position of the fibres representing the longitudinal reinforcement steels are the same with those in the real section (see details of the sections in the contest rules [NEES7story, 2006].

Table 2.3. Material data for the constitutive laws

Concrete parameters			
E_c	24.46GPa	a_2	4.01MPa^{-1}
ν_b	0.2	b_1	1.2
y_{01}	335Pa	b_2	1.335
y_{02}	0.05MPa	β_1	1MPa
a_1	4000MPa^{-1}	β_2	-40Mpa
σ_{fl}	3.5MPa		
Steel parameters			
E_0	200GPa	a_3	0
f_y	450MPa	a_4	0
b	0.0138		

2.1.6 Stiffness of the shaking table

The shaking table is modelled using 4 linear Bernoulli beam elements. The bending stiffnesses of the beams are tuned according to the rotational stiffnesses provided by the

official contest rules.

2.1.7 Numerical strategy

The classical Newmark time integration scheme is used for the calculations assuming a constant variation of the acceleration ($\gamma = 0.5$ and $\beta = 1/4$). The secant Newton-Raphson strategy is chosen and the Rayleigh damping coefficients have been adjusted to ensure a value on 2% on the first and the fourth mode. $P-\delta$ effects are neglected and for computational reasons the 4 dynamic motions (EQ1, EQ2, EQ3, EQ4) have been launched independently (the structure is considered undamaged at the beginning of each loading).

2.2 EXPERIMENTAL DATA AND BLIND RESULTS USING TIMOSHENKO MULTIFIBER BEAMS

The maximum predicted and measured overturning moments, story shear forces, lateral displacements, floor accelerations, inter-story drift ratios, for each level and for the 4 motions (EQ1, EQ2, EQ3 and EQ4) are presented in Figure 2.4, Figure 2.5, and Figure 2.6. The overturning moment M_i at the stage i as well as the story shear force V_i are evaluated thanks to the accelerations of each level (equations 2.1 and 2.2):

$$M_i = \sum_{k=i+1}^{7} \left(M_{wk} + M_{fk}\right) \ddot{u}_{Yk} \left(X_k - X_i\right) \tag{2.1}$$

$$V_i = \sum_{k=i+1}^{7} \left(M_{wk} + M_{fk}\right) \ddot{u}_{Yk} \tag{2.2}$$

Where $\ddot{u}_{Yk}$ is the horizontal acceleration according to Y axis of node k, M_{wk} and M_{fk} the masses and X_k is the height (according to X axis) of node k, with $i \in [0;6]$

The inter-story drift ratio for the story between the nodes i and $i+1$ ($ID_{i,i+1}$) is calculated according to equation (2.3):

$$ID_{i,i+1} = \frac{u_{Yi+1} - u_{Yi}}{X_{i+1} - X_i} \tag{2.3}$$

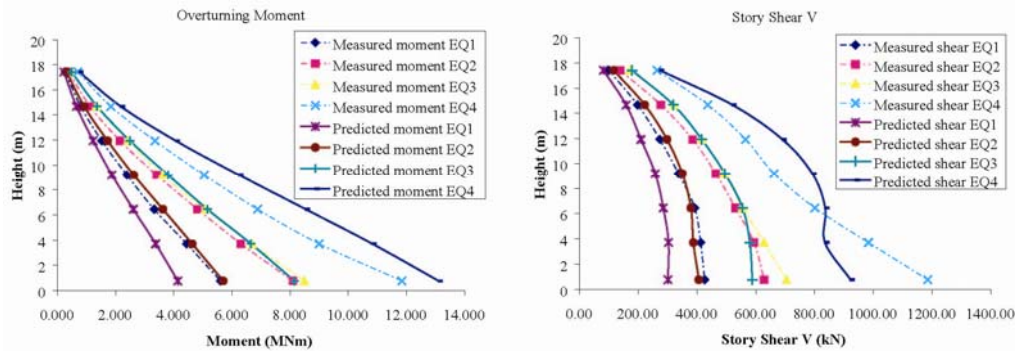

Figure 2.4. Maximum overturning moments and story shear forces at different levels of the structure for the 4 sequences. Experimental (dotted lines) and numerical results (continuous lines).

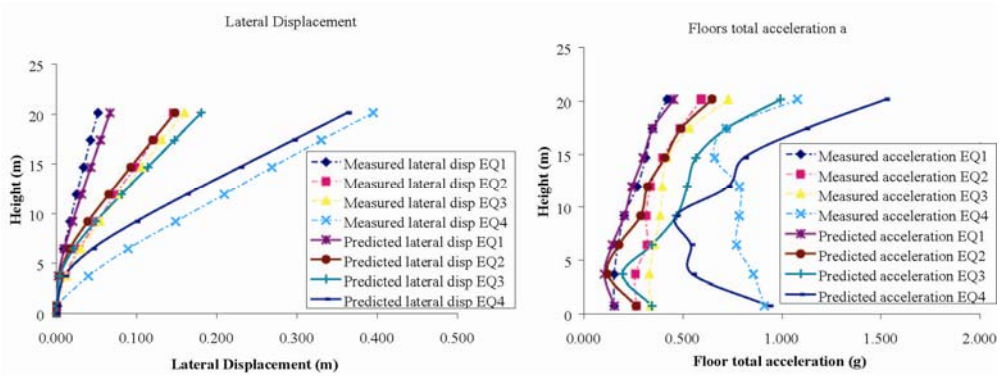

Figure 2.5. Maximum lateral displacements and accelerations at different levels of the structure for the 4 sequences. Experimental (dotted lines) and numerical results (continuous lines).

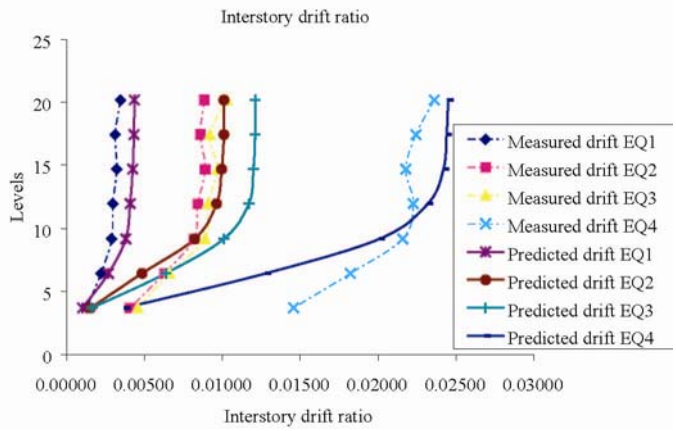

Figure 2.6. Maximum inter-story drift ratios in the structure for the 4 sequences. Experimental (dotted lines) and numerical results (continuous lines).

The calculated response is generally close to the experimental behaviour. Overturning moments and shears are underestimated for EQ1 and EQ2 whereas they are overestimated for EQ4. Lateral displacements are generally close to the experimental ones with values underestimated for EQ4.

These differences come from the fact that the 4 dynamic motions have been launched independently in the numerical model. Another reason is the following: In the experiment, during the EQ4 sequence, a plastic hinge was formed at the first story (at 0 level) (see the measured deformed shape in Figure 2.5). Indeed, in this figure one can observe an angular point present at the base of the structure (at 76cm (30in) height). On the contrary, in the numerical model, damage is concentrated in levels 0 and 1 (Figure 2.7) and so the predicted angular point is positioned higher. This is due to the fact that the continuity of the reinforcement bars between levels 0 and 1 has not been considered in the numerical model. This lack of steel at the junction of the two levels generated a distribution of cracks and damage on both levels. This will be clearly shown in paragraph 2.3.1.

The time history of the calculated and experimental lateral displacements at the top of the structure for the EQ1 and the EQ4 sequences are presented in Figure 2.8. Simulation predicts satisfactory the maximum displacement for both sequences, nevertheless, there is a shift between the curves especially, for EQ1.

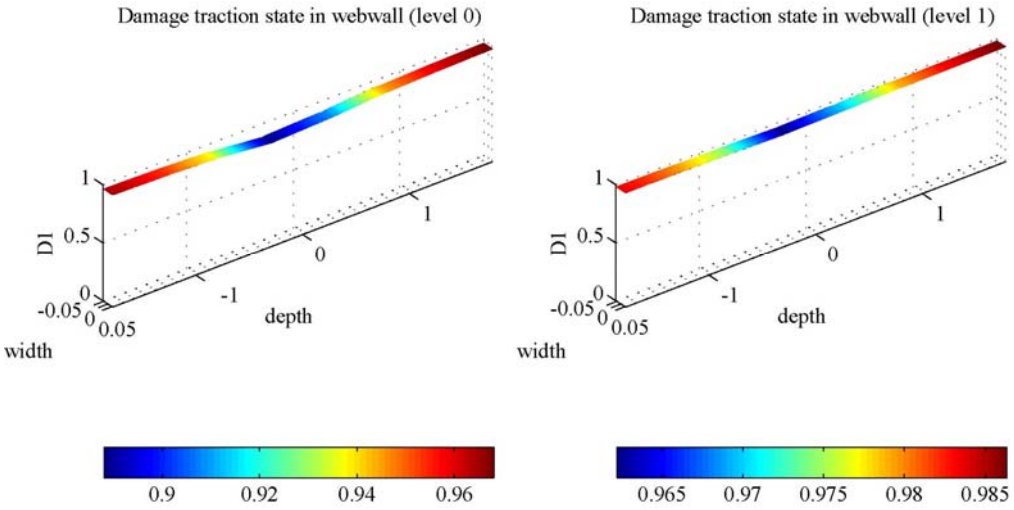

Figure 2.7. State of damage in concrete due to traction at levels 0 and 1 (EQ1).

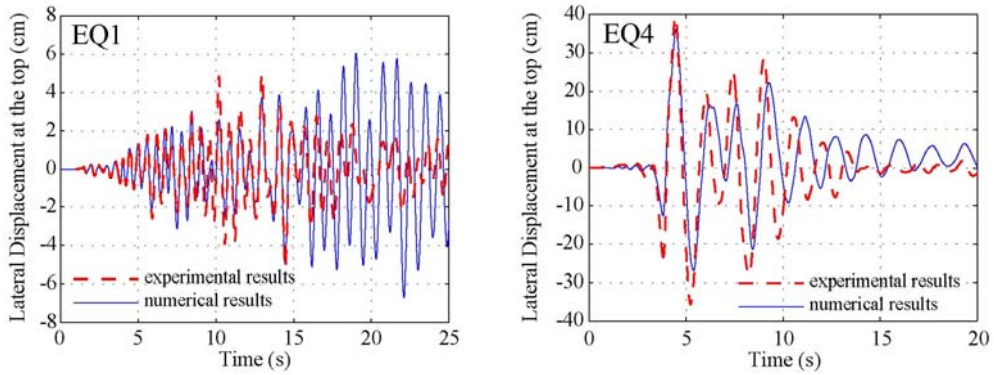

Figure 2.8. Lateral displacements at the top versus time for EQ1 and EQ4. Experimental (dashed lines) and numerical results (continuous lines).

2.3 IMPROVEMENTS OF THE INITIAL MODELING

2.3.1 Considering the continuity of steels at the junction of levels 0 and 1

Reinforcement bars have been added at the numerical model at the junction between levels 0 and 1. The role of these steels is to make stronger the link between the 2 levels (where the width of the section is reduced from 20cm (8in) to 15cm (6in)). This new model leads to a more realistic distribution of damage presented in Figure 2.9.

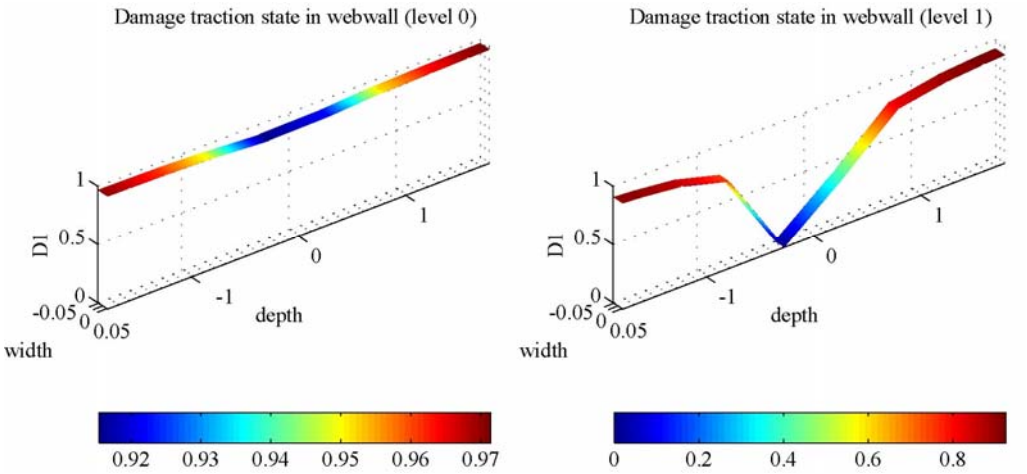

Figure 2.9. State of damage in concrete due to traction for the modified structure at levels 0 and 1 considering continuity of steels (EQ1).

2.3.2 Considering new material and damping data

According to right picture of Figure 2.8, it is clear that the frequency of the numerical model is lower than the experimental one. In order to improve the numerical response the following material parameters have been changed: The concrete ultimate stress in traction f't is not known precisely. A new value is chosen equal to $f'_t = 4MPa\ (= 0.57ksi)$. The steel yield stress f_y can be increased according to the values given in the contest rules. The new value is chosen equal to $f_y = 500MPa\ (= 72.5ksi)$. The last point concerns the coefficients of the Rayleigh damping. The new damping ratio applied to the first and the fourth modes is taken equal to 2.2%. Moreover the continuity of steels is also taken into account. Comparison between the new numerical results and the experimental ones for EQ1 and EQ4 sequences in terms of the lateral displacements at the top of the structure is given in Figure 2.10. The numerical curves are now in phase with the experimental ones and the peaks are correctly reproduced. The pattern of the damage state at the end of the motion EQ1 is given in Figure 2.11. One can see that the damage at level 1 is now decreased and so the plastic hinge is concentrated at level 0 (to be compared with the damage patterns in Figure 2.7 and Figure 2.9).

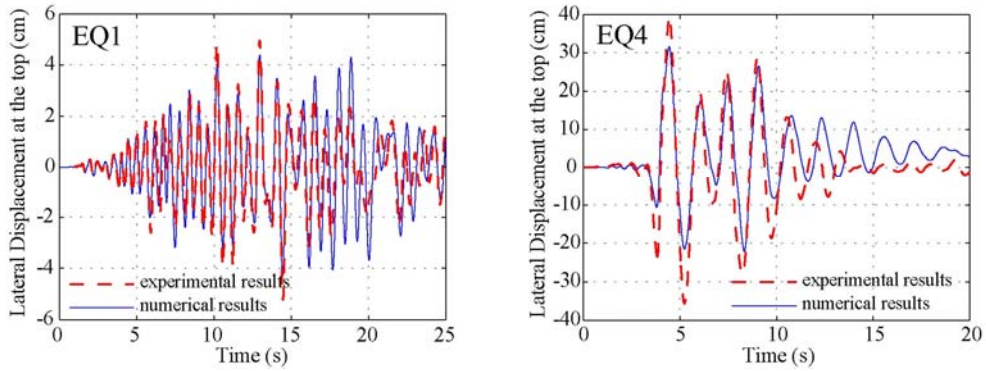

Figure 2.10. Lateral displacements at the top versus time for EQ1 and EQ4. Experimental (dashed lines) and numerical results (continuous lines) for the modified structure considering new material and damping data and the continuity of steels.

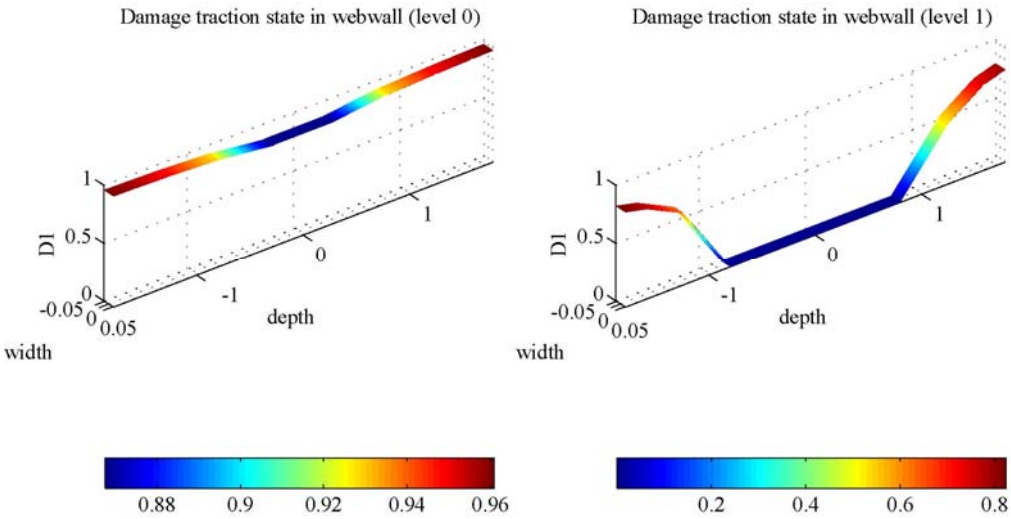

Figure 2.11. State of damage in concrete due to traction for the modified structure at levels 0 and 1 considering new material and damping data and the continuity of steels (EQ1).

2.4 CONCLUSIONS ABOUT THE EMBEDDED STRUCTURE

As demonstrated throughout these results, the modelling strategy based on Timoshenko multifiber beam elements and constitutive laws within the framework of damage mechanics and plasticity is able to reproduce with good approximation the global response of the seven story building and qualitatively the distribution of damage (blind calculations). Moreover, this simplified approach helps reducing computational costs (one loading sequence takes only a couple of hours with Matlab). Some improvements were obtained by modelling correctly the continuity of the reinforcement bars and by adjusting some material and damping parameters. It appears now possible to use this kind of modelling strategy to investigate numerically the behaviour of a wider variety of configurations that is practically impossible to study experimentally. Following this idea, in the next part of this report we investigate numerically the influence of different boundary conditions namely a) SSI using different types of soils and b) base isolator devices.

3.NUMERICAL MODELING OF THE SEVEN-STORY BUILDING CONSIDERING DIFFERENT BOUNDARY CONDITIONS

The numerical results presented in this section are divided into 2 parts:

- Simulations considering SSI for different types of soils;
- Simulations considering the influence of base isolator devices.

3.1 SIMULATIONS CONSIDERING SOIL-STRUCTURE INTERACTION

The structure used for numerical simulations is the same as before but this time it is considered simply posed on the macro element developed in [Grange *et al.,* 2006a], [Grange *et al.,* 2007a], [Grange *et al.,* 2007b]. In other words, the structure has now a rigid shallow and circular foundation simply posed on the soil. The diameter of the footing is equal to $2R=D=4$m and corresponds to 2 rectangular footings with the dimensions given in Figure 3.1. The centre of the foundation is located below the gravity centre of the structure (at 2m from the edge of the flange wall).

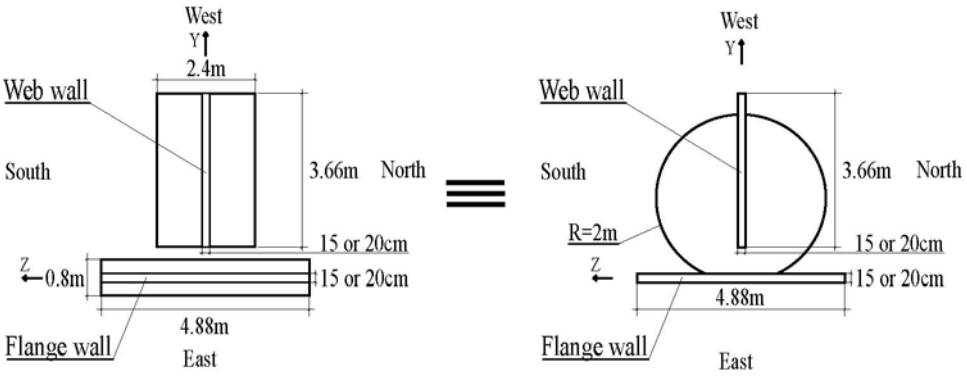

Figure 3.1. Geometrical characteristics of the foundation.

3.1.2 Types of soils used for the simulations

Different types of soils are considered in the simulations presented hereafter. Their characteristics are defined in Table 3.1. All soils have a density $\rho = 1900 kg/m^3$ and a Poisson coefficient $\nu = 0.4$.

Table 3.1. Characteristics of the soils used for SSI simulations

Soil reference	Shear Modulus G_0 and shear wave velocity V_s	cohesion c and friction angle φ	Stiffness of the system "soil/ circular foundation" [Gazetas, 1991]	ultimate compressive stress q_{max}
Soil 1: very low characteristics (class S_2)	V_s = 30m/s G_0 = 1.71MPa	c_u = 30kPa φ_u = 0	$K_{\theta\theta}$ = 60.8MNm/rad K_{zz} = 22.8MN/m K_{hh} = 17.1MN/m	q_{max}= 0.20MPa
Soil 2: low characteristics (class S_1)	V_s = 100m/s G_0 = 19MPa	c_u = 35kPa φ_u = 0	$K_{\theta\theta}$ = 675.5MNm/rad K_{zz} = 253.3MN/m K_{hh} = 190MN/m	q_{max}= 0.234MPa
Soil 3: average characteristics (class D)	V_s = 175m/s G_0 = 58.18MPa	c' = 15kPa φ' = 30°	$K_{\theta\theta}$ = 2068MNm/rad K_{zz} = 775.7MN/m K_{hh} = 581.8MN/m	q_{max}= 1.05MPa
Soil 4: good characteristics (class C)	V_s = 300m/s G_0 = 171MPa	c' = 30kPa φ' = 30°	$K_{\theta\theta}$ = 6080MNm/rad K_{zz} = 2280MN/m K_{hh} = 1710MN/m	q_{max}= 1.7MPa
Soil 5: very good characteristics (class B)	V_s = 400m/s G_0 = 304MPa	c' = 30kPa φ' = 35°	$K_{\theta\theta}$ = 10808MNm/rad K_{zz} = 4053MN/m K_{hh} = 3040MN/m	q_{max}=2.88MPa
Soil 6: rock (class A) with elastic stiffness of the experimental shaking table	V_s > 800m/s		$K_{\theta\theta}$ = 18302MNm/rad K_{zz} = infinity K_{hh} = infinity	q_{max}= infinity

The classification used in Table 3.1 is taken from [Davidovici, 1999] and Eurocode 8 [EC8, 2005]. The criterion for the classification is the shear wave velocity in the soil (class A: solid bed rock to class S_2: soil with very low characteristics). Elastic stiffnesses are calculated thanks to the dynamic impedances given in [Pecker, 1984], [Gazetas 1991] for a circular shallow foundation according to:

$$\begin{cases} K_{hh} = \dfrac{8G_0R}{2-\nu}\left(1+0.5\dfrac{R}{H}\right) \\ K_{\approx\approx} = \dfrac{4G_0R}{1-\nu}\left(1+1.28\dfrac{R}{H}\right) \\ K_{\theta\theta} = \dfrac{8G_0R^3}{3(1-\nu)}\left(1+0.17\dfrac{R}{H}\right) \end{cases} \tag{3.1}$$

H being the distance of the layer of a soil with very good characteristics (bed rock) from the surface. For the calculations presented in this report *H* is considered very big which permits to cancel the last term of the equation.

The ultimate compression stress is given by the relationship provided in [Philipponnat *et al.,* 2003] adapted for a circular footing:

$$q_{\max} = \frac{0.6}{2}\gamma B N_\gamma + q_0 N_q + 1.3cN_c \tag{3.2}$$

Where N_γ is the surface term, N_q the term depending on the depth of the foundation, and N_c the cohesion term. For our calculations the foundation is considered on the soil surface and so $q_0 = 0$. The relations allowing calculating N_γ, N_q and N_q are given in [Caquot *et al.,* 1966]. They depend only to the cohesion *c* of the soil and the friction angle φ.

3.1.3 Numerical results

We present in this section the numerical results of the NEES structure considering 6 different soils according to Table 3.1 for the loading sequence EQ4. The modified numerical model is used considering the new material and damping data and continuity of steels. Figure 3.2 shows the maximum overturning moments, story shears, lateral displacements, inter-storey drift ratios and floor accelerations for each level. The SSI influence is compared with the behaviour of the original structure embedded in the shaking table (see section 2). The internal forces presented here (overturning moments and story shears) are calculated at the base of the web wall only. This is the reason why they differ from those presented in section 2 (where internal forces are given for the whole structure, calculated by multiplying the accelerations with the masses).

As expected, SSI isolates the structure. Indeed, when looking at Figure 3.2 and Figure 3.3 overturning moments and story shears are reduced. For soils with low characteristics this reduction is more significant. More particular, for soils 1 and 2 numerical predictions provide the location of the maximum moment not longer at the base of the structure but

near the level 2.

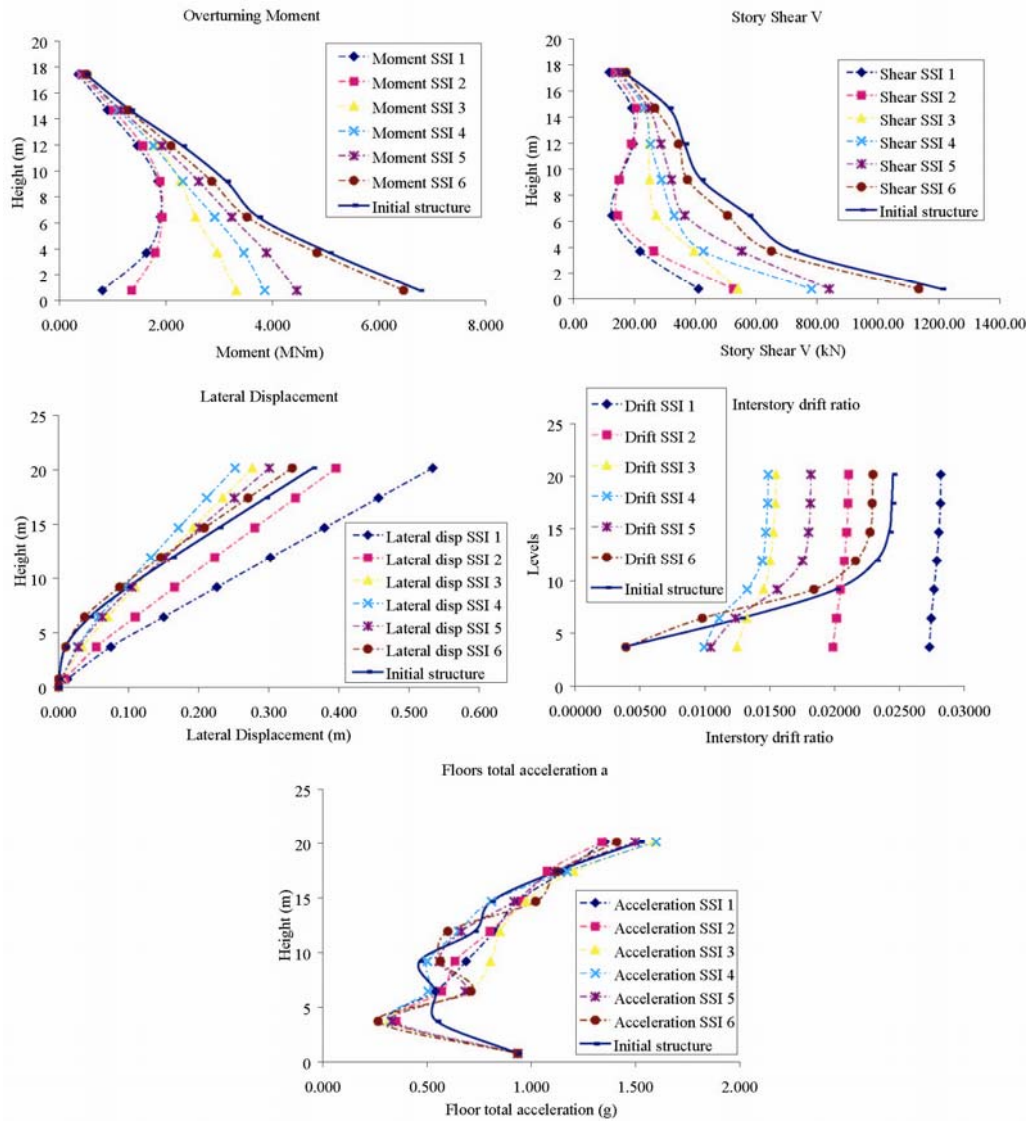

Figure 3.2. Maximum overturning moments, story shears, lateral displacements, drifts and floor accelerations for 6 different soils and comparison with the structure embedded on the shaking table.

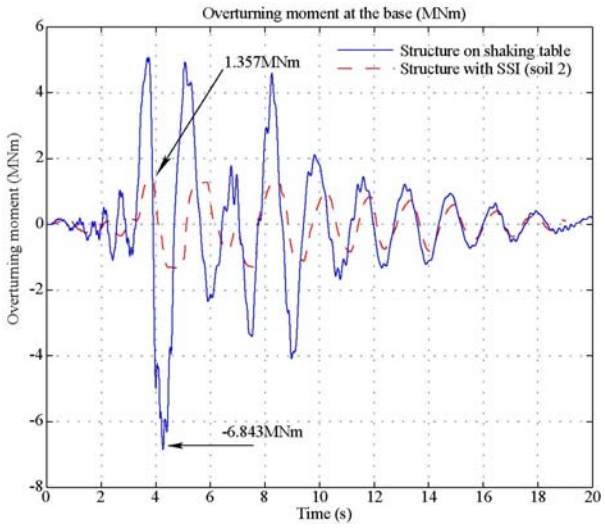

Figure 3.3. Overturning moment at the base versus time for the embedded structure and the structure considering SSI (soil 2).

The reason of this is the high participation of the first 2 modes in the behaviour of the structure. This can be identified by proceeding to the modal decomposition of the moments according to the Karhunen-Loéve method [Gutiérrez *et al.*, 2000]. Figure 3.4 shows the static modal shape and the modal participation and the time history of the moment's projection on the modal space for the structure considering SSI (soil 2). It is obvious that the first two modes contribute a lot to the behaviour of the structure. This is also shown by reconstructing the moment time history at the base of the structure. Only the first 2 modes are necessary to reproduce accurately the original moment time history (Figure 3.5).

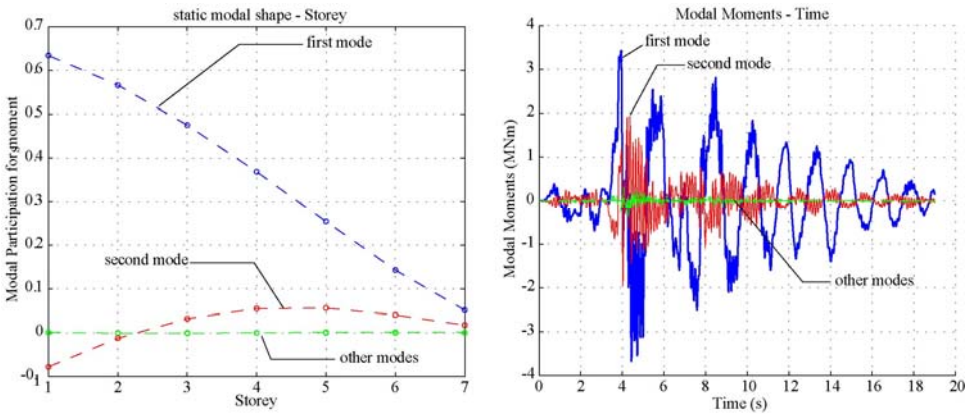

Figure 3.4. Static modal shape of the moments and modal moments versus time for the structure considering SSI (soil 2).

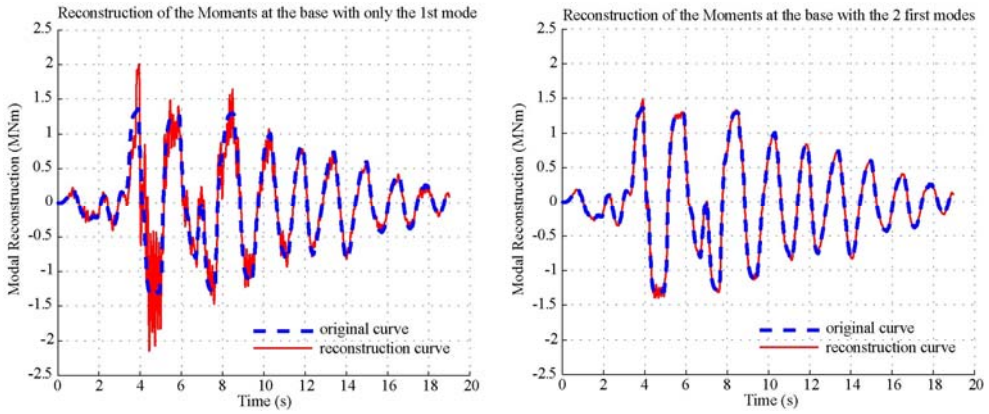

Figure 3.5. Reconstruction of the moments at the base of the structure considering SSI using only the first mode or the first 2 modes (soil 2).

Figure 3.2 shows that the lateral displacements at the top are higher for the structure on soils with low characteristics (1 and 2) than for the embedded structure. Nevertheless, they are lower for soils 3, 4 and 5. This can be explained looking at Figure 3.6. The peaks of the two curves are not happening at the same time and so it is not obvious to predict which of the two structures will have the higher displacement. Moreover, by applying the Karhunen-Loéve method to the displacements one can see that the first mode is preponderant compared to the others (Figure 3.7 and Figure 3.8). That's why the deformed shape of the structure on soil 2 corresponds to the first mode on Figure 3.2.

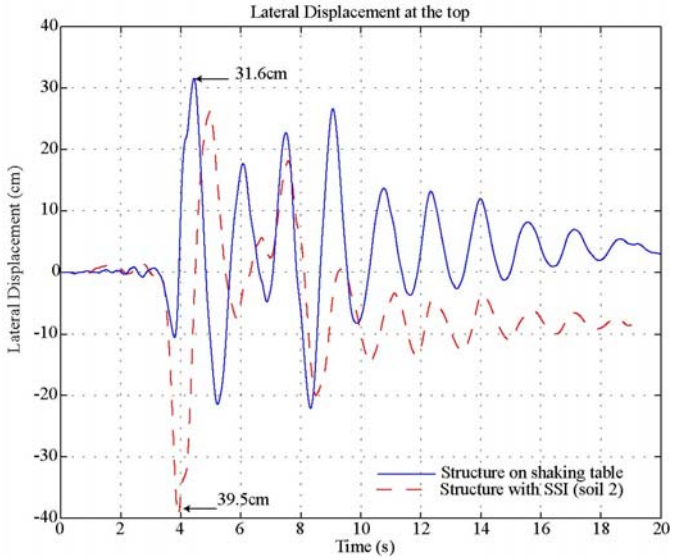

Figure 3.6. Lateral displacement at the top versus time for the embedded structure and the structure considering SSI (soil 2).

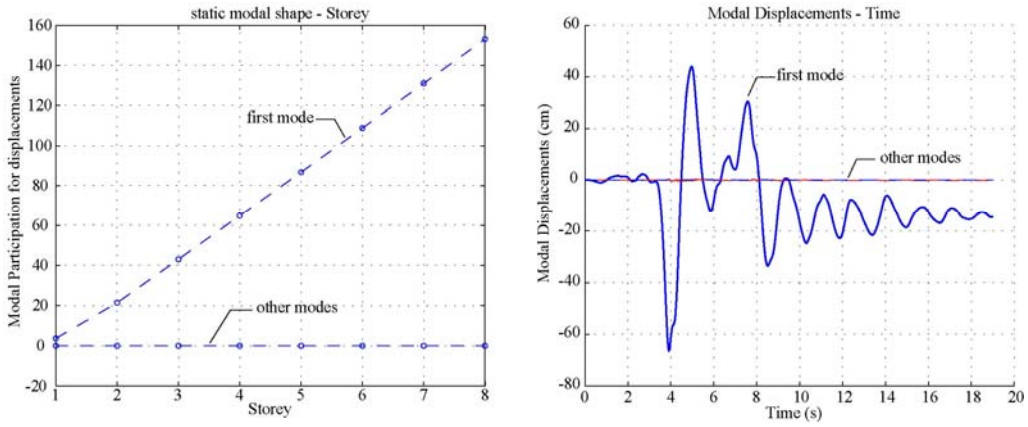

Figure 3.7. Static modal shape of the displacements and modal displacements versus time for the structure considering SSI (soil 2).

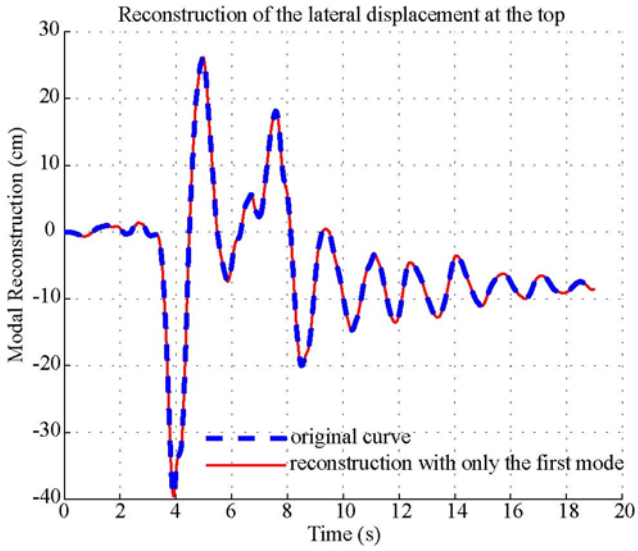

Figure 3.8. Reconstruction of the lateral displacements at the top of the structure considering SSI using only the first mode (soil 2).

Figure 3.2 shows also that the inter-story drift ratio is quasi constant for soils 1 and 2. This is typical for a structure that stays elastic during the entire loading sequence. This is verified in Figure 3.9 presenting the damage distribution at levels 0 to 3.

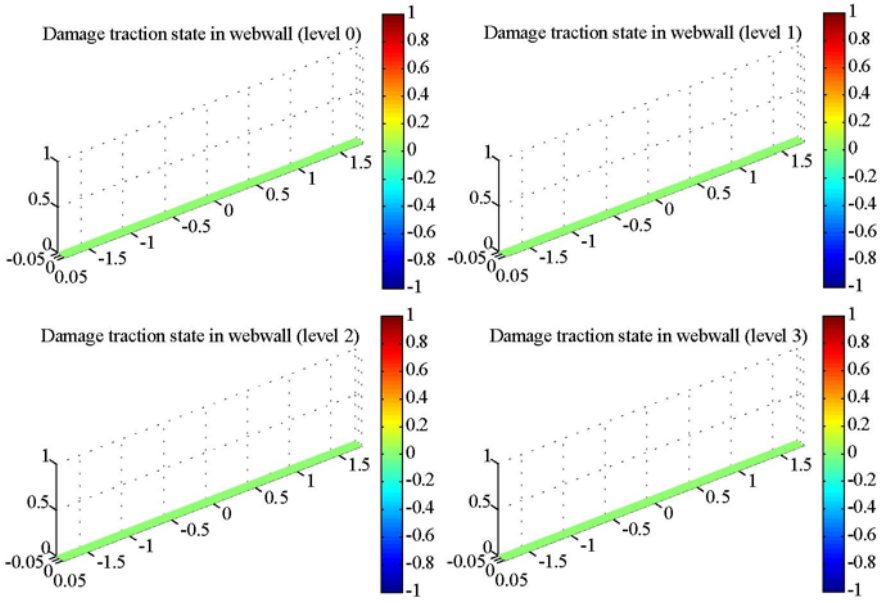

Figure 3.9. State of damage in concrete due to traction for the structure considering SSI at levels 0 to 3 (soils 1 and 2).

Figure 3.10, Figure 3.11, Figure 3.12, Figure 3.13 and Figure 3.14 show the evolution of damage at the 4 first levels for soils 3, 4, 5 and 6 and for the embedded structure. It is clear that better the soil more important is the damage. It seems also that the different flexibilities of the soils have not the same influence on the behaviour of the structure. Indeed, damage is not reduced at all the levels; it stays high at level 2 even for soils with low characteristics. The influence of the second mode can explain this phenomenon. Another reason is the fact that damage in traction grows more rapidly in sections where compression forces - due to the weight of the structure - are low (the ultimate moment is lower at the top of the structure than at lower levels).

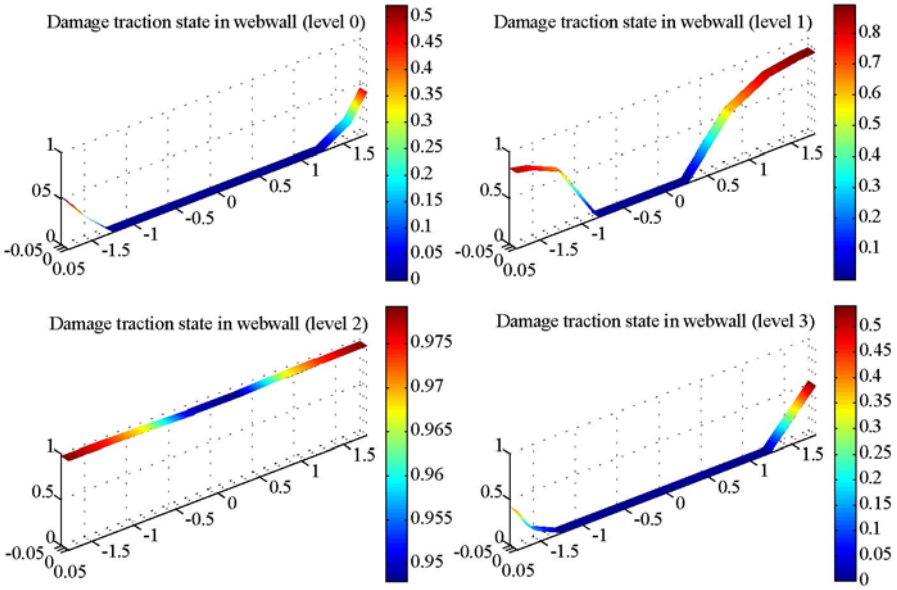

Figure 3.10. State of damage in concrete due to traction for the structure considering SSI (soil 3).

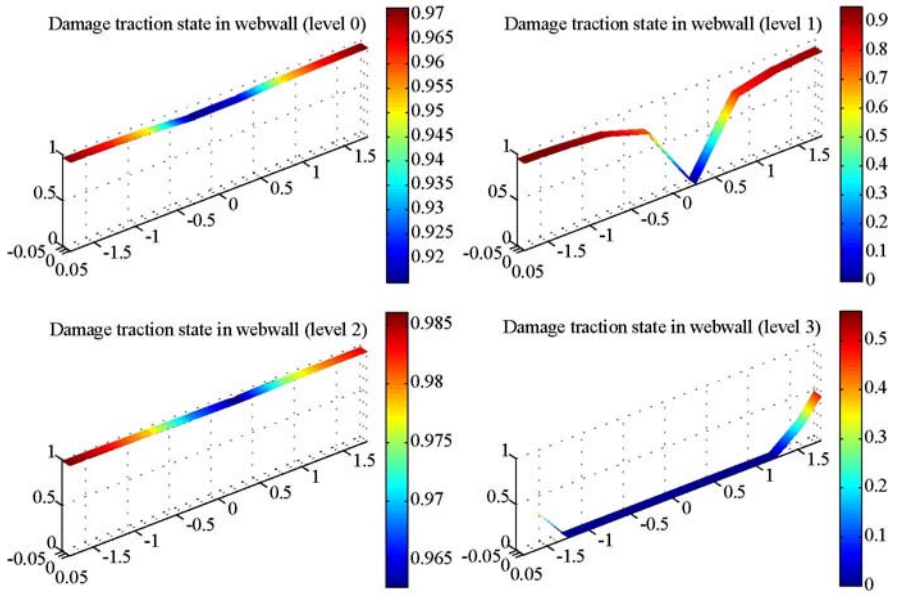

Figure 3.11. State of damage in concrete due to traction for the structure considering SSI (soil 4).

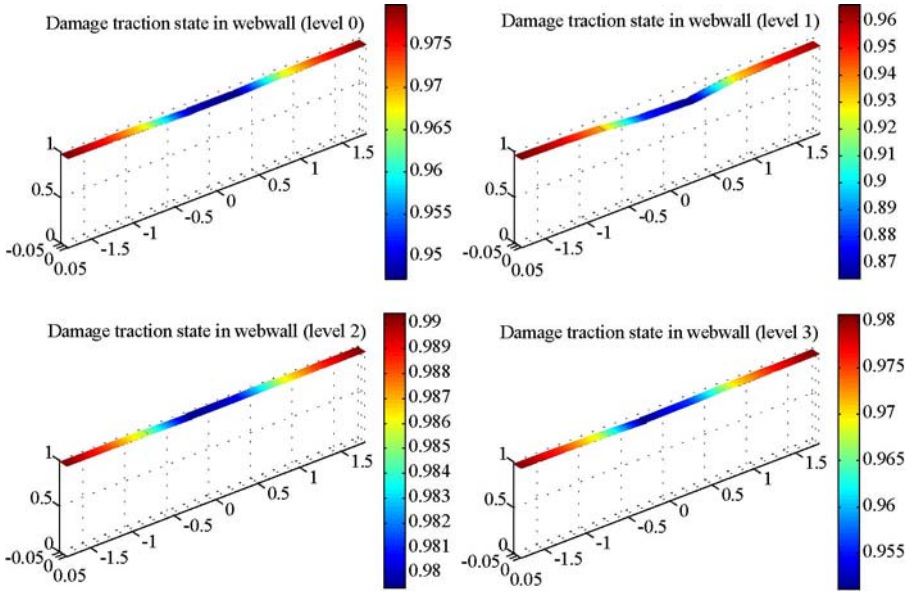

Figure 3.12. State of damage in concrete due to traction for the structure considering SSI (soil 5).

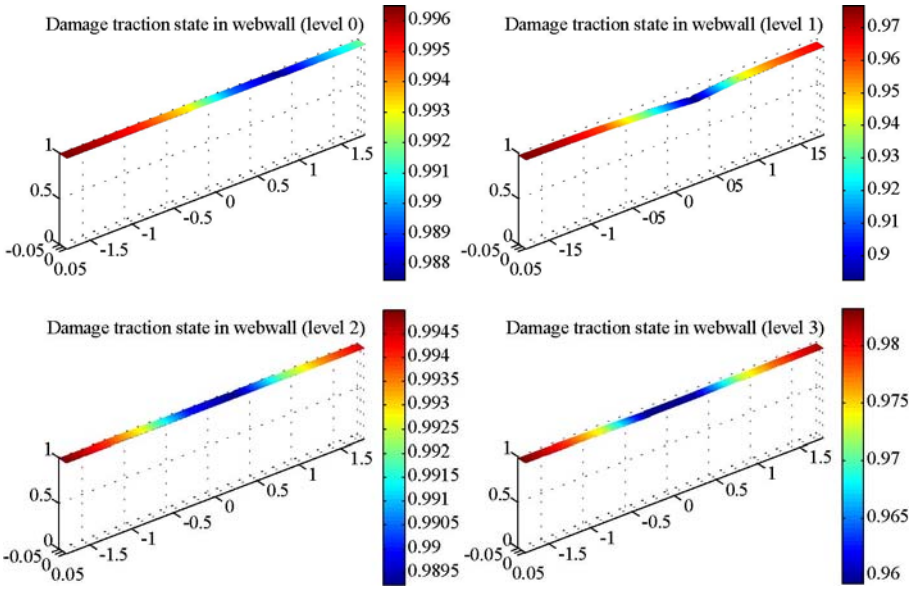

Figure 3.13. State of damage in concrete due to traction for the structure considering SSI (soil 6).

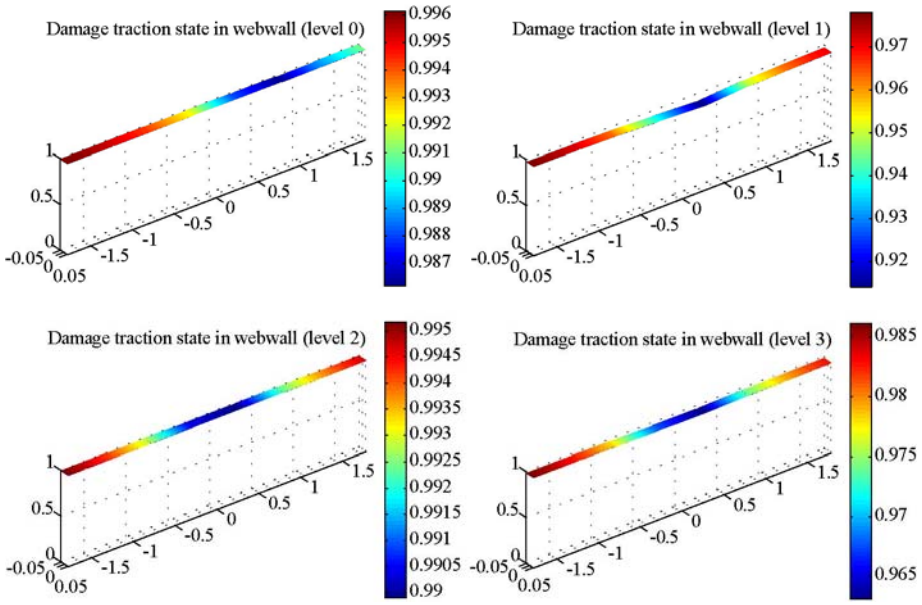

Figure 3.14. State of damage in concrete due to traction for the structure embedded on the shaking table.

3.2 SIMULATIONS CONSIDERING THE INFLUENCE OF BASE ISOLATOR DEVICES

Structural isolation is based on the idea of decoupling the building from the horizontal components of the earthquake. Numerical simulations follow in order to show the influence of base isolator devices in the behaviour of the NEES structure.

Classical base isolators dissipate energy only through shear deformation thus the rotational stiffness at the base of the structure is considered infinite in the numerical model. The macro element [Grange *et al.*, 2006a] is used to simulate the laminated rubber bearings based isolators devices described in [Chung *et al.,* 1999] and represented in Figure 3.15.

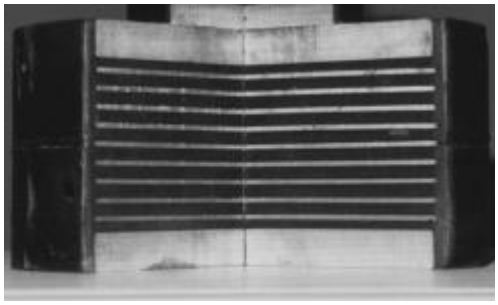

Figure 3.15. Cross-section of base isolator [Chung *et al.*, 1999].

The details of the base isolators are recalled on Figure 3.16. The particularity of this kind of device is that the effective stiffness is quite constant even for large displacements [Dolce *et al.*, 2006], a characteristic that can be easily reproduced by the macro element. Figure 3.17 shows the results of the numerical simulations using the macro element compared to the experimental curves for the ¼ scaled specimens provided in [Chung *et al.*, 1999].

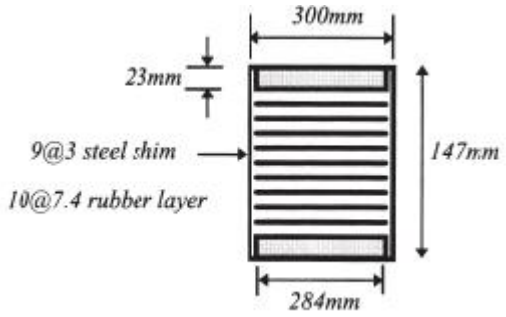

Figure 3.16. Details of the base isolator [Chung *et al.*, 1999].

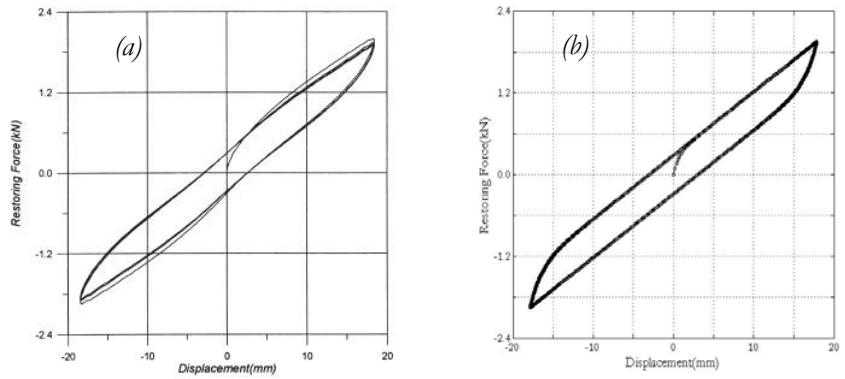

Figure 3.17. Base isolator - Relationship between horizontal force and displacement: (a) Experimental results, and (b) numerical results using the macro element (¼ scaled specimens).

In order to reproduce the influence of the base isolators on the NEES structure 3 scaled 1 devices are introduced into the numerical model of the web wall. Based on the experimental curves presented in Figure 3.17 extrapolations are assumed to simulate the behaviour of the scaled 1 devices. Simulations are performed for the EQ2 earthquake [NEES7story, 2006]. The maximum displacements at each story of the structure are presented in Figure 3.18.

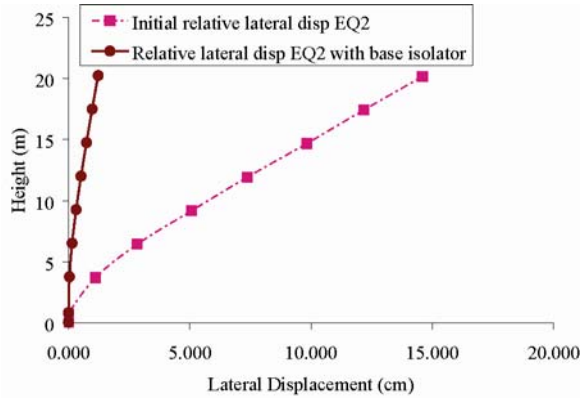

Figure 3.18. Comparison between the maximum relative displacements at different levels of embedded structure and the structure with base isolator devices (EQ2).

It is clear that the relative displacements of the isolated structure are highly reduced. The inter-story drift ratio is near to 0. This indicates that the storeys oscillate in a quasi rigid body mode and that no damage is developed in the structure (verified also numerically). Moments and shears are also found reduced.

4. CONCLUSION AND WAY FORWARD

As demonstrated at the first part of this report, the modelling strategy based on Timoshenko multifiber beam elements and constitutive laws within the framework of damage mechanics and plasticity is able to reproduce with good approximation the global response of the seven story building and qualitatively the distribution of damage (blind calculations). Moreover, this simplified approach helps reducing computational costs (one loading sequence takes only a couple of hours with Matlab). Some improvements were obtained by modelling correctly the continuity of the reinforcement bars and by adjusting some material and damping parameters.

Timoshenko multifiber beam elements coupled with the new macro element are used at the second part of the report to investigate numerically the behaviour of the NEES structure considering a wider variety of boundary conditions. More specifically:

- Simulations of the non linear behaviour of the NEES structure on a circular rigid foundation submitted to dynamics loadings are satisfactory. Results are presented for a large variety of soils. It is shown that SSI isolates the structure: global forces and damage in concrete are significantly reduced. Results can however be different for lateral displacements. A decrease in the properties of the soil does not induce necessarily an increase of the lateral displacements but can lead to an increase of the influence of higher order modes…

- Simulations of the non linear behaviour of the NEES structure on base isolator devices show a great influence on the final deformed shape. Even though high absolute displacements occur at the base of the structure inter-story drift is close to 0 and damage and moments are found decreased.

REFERENCES

BAEL91, [2000] *Règles techniques de conception et de calcul des ouvrages et constructions en béton armé suivant la méthode des états-limites*. Eyrolles, Paris, France.

Caquot, A., and Kérisel, J., [1966]. *Traité de mécanique des sols*. Gautiers-Villars, France.

Chung, W.J., Yun, C.B., Kim, N.S., Seo, J.W., [1999] "Shaking table and pseudodynamic tests for the evaluation of the seismic performance of based isolated structure", *Engineering Structures*, Vol. 21, pp 365-379.

Crémer, C. [2001] "Modélisation du comportement non linéaire des fondations superficielles sous séismes", PhD Thesis, LMT Cachan - ENS Cachan, France.

Davidovici, V., [1999], *La construction en zone sismiqu*e, Le Moniteur, France.

Dolce, M., Cardone D., and Ponzo, F.C., [2006] "Shaking-table tests on reinforced concrete frames with different isolation systems", *Earthquake Engng Struct. Dyn.* (in press) DOI: 10.1002/eqe.642.

EC8, [2005] NF P 06 030-1, NF EN 1998-1, Eurocode 8 : Calcul des structures pour leur résistance aux séismes. Partie 1 : Règles générales, actions sismiques et règles pour les bâtiments, Septembre, AFNOR.

Filippou, F.C., Popov, E.P., Bertero, V.V., [1983] "Effects of bond deterioration on hysteretic behavior of reinforced concrete joints". *Technical report EERC-83/19, Earthquake Engrg. Res. Ctr.* Univerity of California, Berkeley.

Filippou, F.C. and Constandines, M. [2004] *FedeasLab Getting Started Guide And Simulations Examples*. Dpt of civil and env. Engng. UC Berkeley.

Gazetas, G. [1991] "Foundations vibrations". In *Foundation Engineering Handbook*, Chapter 15. Fang H-Y (ed.), van Nostrand Reinhold: New York.

Grange S., Kotronis P., Mazars J., [2006a] "Advancement of simplified modelling strategies for 3D phenomena and/or boundaries conditions for base-isolated buildings or specific soil-structure interactions", Deliverable 67, European Contract LESSLOSS, Project No.: GOCE-CT-2003-505488, Risk Mitigation for Earthquakes and Landslides, Sixth Framework Programme, 2006 (http://hal.archives-ouvertes.fr/hal-00102513).

Grange, S., Mazars, J., and Kotronis, P., [2006b] "Seven-story building-slice earthquake blind prediction contest: a simplified modeling using multifiber timoshenko beams", *Workshop and Seminar on Analytical Modeling of Reinforced Concrete Walls for Earthquake Resistance,* San Diego, USA-California, December 15-16.

Grange, S., Kotronis, P., and Mazars, J., [2007a] "A 3d macro-element for soil-structure interaction", *International Journal for Numerical and Analytical Methods in Geomechanics*, submitted to publication.

Grange, S., Kotronis, P., and Mazars, J., [2007b] "3d macro element for soil structure interaction", *4th International Conference on Earthquake Geotechnical Engineering*, Thessaloniki, Grèce, June 25-28 (in press).

Gutiérrez, E., and Zaldivar, J.M., [2000] "The application of Karhunen-Loéve, or principal component analysis method, to study the non-linear seismic response of structures », *Earthquake Engng Struct. Dyn.*, 29: 1261-1286.

Kotronis, P., and Mazars, J., [2005]. "Simplified modelling strategies to simulate the dynamic behaviour of r/c walls", *Journal of Earthquake Engineering*, 9(2):285–306.

La Borderie, C., [1991] "Phénomènes unilatéraux dans un matériau endommageable: modélisation et application l'analyse des structures en béton", Phd thesis, Université Paris 6.

Mazars, J., Kotronis, P., Ragueneau, F., and Casaux, G., [2006]. "Using multifiber beams to account for shear and torsion. applications to concrete structural elements", *Computer Methods in Applied Mechanics and Engineering*, 195(52):7264–7281.

Menegoto, M., and Pinto, P., [1973]. "Method of analysis of cyclically loaded reinforced concrete plane frames including changes in geometry and non-elastic behaviour of elements under combined normal force and bending". In IABSE Symposium on resistance and ultimate deformability of structures acted on by well-defined repeated loads, final report, Lisbon, 328p.

NEES7story, [2006] NEES/UCSD seven-story building-slice earthquake blind prediction contest http://nees.ucsd.edu/7Story.html

Pecker, A. [1984] *Dynamique des sols*. Presse, ENPC, Paris, France.

Philipponnat, G., and Hubert, B., [2003] *Fondations et ouvrages en terre*, Eyrolles, Paris, France.